



Complex dynamics of a particle in an oscillating potential field

BARNALI PAL¹, DEBJIT DUTTA^{2,*} and SWARUP PORIA¹

¹Department of Applied Mathematics, University of Calcutta, 92 Acharya Prafulla Chandra Road, Kolkata 700 009, India

²Department of Basic and Applied Science, National Institute of Technology, Arunachal Pradesh 791 112, India

*Corresponding author. E-mail: debjitdutta.math@gmail.com

MS received 15 August 2015; revised 9 March 2017; accepted 6 April 2017; published online 25 July 2017

Abstract. In this paper, the classical problem of the motion of a particle in one dimension with an external time-dependent field is studied from the point of view of the dynamical system. The dynamical equations of motion of the particle are formulated. Equilibrium points of the non-oscillating systems are found and their local stability natures are analysed. Effect of oscillating potential barrier is analysed through numerical simulations. Phase diagrams, bifurcation diagrams and variations of largest Lyapunov exponents are presented to show the existence of a wide range of nonlinear phenomena such as limit cycle, quasiperiodic and chaotic oscillations in the system. Effects of nonlinear damping in the model are also reported. Analysis of the physically interesting cases where damping is proportional to higher powers of velocity are presented for the sake of generalizing our findings and establishing firm conclusion.

Keywords. Time-dependent potential; Lyapunov exponents; bifurcation; equilibrium points; integrable systems.

PACS Nos 02.10.Yn; 02.30.Ik; 02.60.Cb; 05.45.–a

1. Introduction

The investigation of problems described by potential wells or barriers where the particles are subjected to the effect of noise or the barriers are assumed to move in time is a subject of great interest for many researchers from the last decades [1–10]. After the pioneering work of Buttiker and Landauer [11] on tunnelling through a time-dependent potential barrier, interest in the dynamics of a particle in a driven potential has markedly increased. The dynamics of a particle inside an infinite potential box that contains a periodically oscillating barrier [12–14] and the dynamics of a classical particle in a time-dependent oscillating well [7,15] have been received much attention in theoretical and experimental physics [16,17]. It is also interesting to study the problem of a classical particle interacting with a static or time-dependent multiwell potential in the presence of noise. The notion of a time-dependent potential may also be extended to encompass the class of problems known as billiards [18–20]. In particular, the time-dependent Hamiltonian systems lead to significant advances towards a qualitative and quantitative understanding of their behaviour over a long time. In many

cases, the chaotic dynamics of a particle inside the driven potential leads to very interesting phenomena, including power-law distribution for the trapping [15,21], scattering [7] and critical exponents for the average properties of the chaotic sea [22].

It may be recalled that in a few cases it is required to study the classical analogue to characterize quantum mechanical phenomenon well and so in different context [23] significantly a large number of quantum-classical analogies have been studied. However, there are a few purely quantum phenomena such as tunnelling, wave-particle duality, or interference in which classical analogies are quite incapable of giving clear explanation. In particular, the quantum tunnelling can be described in terms of classical physics via mapping that links a complex-valued wave function solution of the time-independent Schrödinger's equation (TISE) with classical behaviour of a pair of uncoupled time-dependent harmonic oscillators. The time-dependent harmonic oscillator equation can be written as

$$\ddot{x} + \Omega^2(t)x(t) = 0. \quad (1)$$

The above equation can be interpreted as the Newton's law of motion for a massive particle in a time-dependent

one-dimensional harmonic potential. Moreover, the time-dependent Hamiltonian corresponding to (1) is

$$H = \frac{p^2}{2m} + \frac{1}{2}m\Omega^2(t)x^2, \quad p = m\dot{x}, \quad (2)$$

where m denotes the mass and x denotes the coordinate of the particle.

It may be noted that most of our knowledge about molecular, atomic and elementary particle physics comes from the analysis of scattering experiments. The potential fields producing the scattering may be the result of one or many particles and may be autonomous or time-dependent. We may infer that the classical and quantum mechanical study of time-dependent Hamiltonian systems are generic and important. The existence of invariants (constants of motion) play an important role in the study of any classical dynamical system. When Hamiltonian is an explicit function of time, it is no longer possible to be an invariant, and this is due to the reflection of the non-conservation of energy. The most widely studied time-dependent Hamiltonian system is the time-dependent harmonic oscillator. In [24], the classical kicked singular oscillator has been extensively studied which is time-dependent. It was studied also partly by Lewis and Leach [25] and Camiz *et al* [26]. Another type of time-dependent potential of the form $Bx^4 - Ax^2 + \Lambda x \cos(\omega t)$ is widely used in both classical and quantum systems. Classical dynamics of a rotating particle under a time-dependent potential has been studied in [27]. In this study, the non-relativistic classical as well as the quantum behaviours of a particle seen from a frame which rotates with a time-dependent angular velocity and subject to time-dependent potentials, has been analysed in detail.

We are motivated to understand the motion of particle in one dimension with space–time-dependent potential field. The Hamiltonian that describes the model is of the type $H(x, p, t) = p^2/2m + V(x, t)$ where x , p and t correspond to the position, momentum coordinates and time respectively. It is important to note that in our case the time-dependent potential $V(x, t)$ is controlled by different control parameters. Change of control parameters may cause a phase transition from integrability (characterized by a constant energy of the particle) to non-integrability (where the particle may be observed either in a chaotic or regular dynamics). The aim of this paper is to show the effects of time-dependent potential field on the dynamics of a particle. It may be noted that parametric excitation is the explicit time-dependent variation of a parameter in a dynamical system. Thus, in the case of parametric excitation, no extra force will appear as an additive term. On the other hand, in the case of direct forcing, some direct additive term will appear in the model. Periodic excitation of the parameters of

a system is also known as modulation of parameter. Therefore, the problem investigated here is much more different from the parametric excitation problem.

Forced Duffing oscillator is one of the most explored nonlinear dynamical systems because it serves as a prototype model for various physical and engineering problems such as particle in a plasma, particle in a forced double well, dynamics of a buckled elastic beam, defect in solids, etc. [28]. Van der Pol–Duffing oscillator mathematical model is used to model cerebrovascular hemodynamics in the presence of arterial aneurysm [29]. Duffing–van der Pol oscillator model can be used to model human brain EEG signal [30]. It is evident that the Van der Pol–Duffing oscillator can be used to model, physical, engineering, biological, neurological and many other systems. The theoretical investigation of the dynamics of a particle moving in an oscillating potential has been an active field of modern research due to its stabilizing effects on dynamical systems [31] and applications in modelling of different behavioural and perceptual states of the brain. Different behavioural and perceptual states of the brain are associated with the oscillatory behaviours of neurons [32] which may be modelled by using Van der Pol–Duffing oscillator with oscillating potential. These facts may motivate us to study oscillators with oscillating potential.

In this paper, we revisit the problem of a classical particle containing a time-dependent potential barrier, seeking to understand some phase-space properties of this system. The orbits of the particle in phase space can be periodic, quasiperiodic or even chaotic, depending on the parameters and the initial conditions of the motion. In §2, models are formulated. Equilibrium points of the model are determined and their linear stability nature are analysed. In §3, numerical simulation results are presented and analysed. Finally, conclusions are drawn in §4.

2. Model

We consider the motion of a particle in one dimension with space–time-dependent potential field. Equation of motion of a particle subjected to the viscous force $-\mu\dot{x}$ in the potential field $V(x, t)$ can be written as [1]

$$\ddot{x} = -\mu\dot{x} - \frac{\partial V}{\partial x}. \quad (3)$$

Here, we consider the space–time-dependent potential field as [33]

$$V(x, t) = \frac{\alpha x^2}{2} + \frac{\beta x^4}{4}$$

$$-\frac{\omega^2 b}{4} \left[-\frac{b}{2} + \cos(\omega t) + \frac{b}{2} \cos(2\omega t) \right] x^2. \tag{4}$$

In [33], this kind of space-quadratic potential has been considered underlying the case of time and space-modulated potential with constant nonlinearities. In particular, this potential is observed in the framework of time-periodic optical superlattice, which is characterized by two distinct frequencies ω and 2ω . In another scenario, it is clear that the depth of the potential well oscillates in time. As the Hamiltonian of the system is time-dependent, the total energy of the particle is not conserved. The Hamiltonian is given by

$$H(p, x, t) = \frac{p^2}{2m} + \frac{\alpha x^2}{2} + \frac{\beta x^4}{4} - \frac{\omega^2 b}{4} \left[-\frac{b}{2} + \cos(\omega t) + \frac{b}{2} \cos(2\omega t) \right] x^2.$$

The Hamiltonian is of the form

$$H(p, x, t) = \frac{p^2}{2m} + V_0(x) + V_1(x)f(t),$$

where $f(t+\tau) = f(t)$ with τ as the period of oscillation of the barrier. Notice that when $V_1 = 0$ and $\mu = 0$ the motion is regular and the energy is conserved.

2.1 Linear damping

Now from eq. (3) we get the equation of motion of a particle under linear damping as

$$\ddot{x} = -\mu\dot{x} - \alpha x - \beta x^3 + \frac{\omega^2 b}{2} \left[-\frac{b}{2} + \cos(\omega t) + \frac{b}{2} \cos(2\omega t) \right] x. \tag{5}$$

Equation (5) can be written as the following coupled set of equations:

$$\begin{aligned} \dot{x} &= y \\ \dot{y} &= -\mu y - \alpha x - \beta x^3 + \left\{ \frac{\omega^2 b}{2} \left(\frac{b}{2} \cos 2z + \cos z - \frac{b}{2} \right) \right\} x \\ \dot{z} &= \omega. \end{aligned} \tag{6}$$

This is the dynamical system corresponding to the motion of a particle in one dimension with space-time-dependent potential. Without oscillation of the potential barrier, the above system reduces to

$$\ddot{x} + \mu\dot{x} - Ax + Bx^3 = 0, \tag{7}$$

where $\mu > 0$ is the damping factor and

$$A = -\left(\alpha + \frac{\omega^2 b^2}{4} \right), \quad B = \beta.$$

This is the famous Duffing equation. We know that the total energy of the system is $E = \frac{1}{2}m\dot{x}^2 + V(x)$. As

$$\frac{dE}{dt} = \dot{x}(\ddot{x} + Bx^3 - Ax) = -\mu\dot{x}^2 \tag{8}$$

the energy is decreasing along all trajectories of system (7) due to damping. Equation (7) can be rewritten as

$$\begin{aligned} \dot{x} &= y, \\ \dot{y} &= Ax - Bx^3 - \mu y. \end{aligned} \tag{9}$$

If $A > 0$ and $B > 0$, then the equilibrium points of the system are $(0, 0)$ and $(\pm\sqrt{A/B}, 0)$. Now, for double-well potential, we take $\alpha < 0$ and $\beta > 0$ and we choose ω, b such that $\alpha > (\omega^2 b^2/4)$. The Jacobian of system (9) is

$$J = \begin{pmatrix} 0 & 1 \\ A - 3Bx^2 & -\mu \end{pmatrix}.$$

The value of the Jacobian matrix at $(0, 0)$ is

$$J = \begin{pmatrix} 0 & 1 \\ A & -\mu \end{pmatrix}.$$

Eigenvalues of the Jacobian matrix are given by

$$\lambda = \frac{-\mu \pm \sqrt{\mu^2 + 4A}}{2}.$$

Clearly, this matrix has two real eigenvalues, one positive and one negative because $A > 0$. Hence, the equilibrium point $(0, 0)$ is a saddle point of system (9). The value of the Jacobian at $(\pm\sqrt{A/B}, 0)$ is

$$J = \begin{pmatrix} 0 & 1 \\ -2A & -\mu \end{pmatrix}.$$

Eigenvalue of the Jacobian matrix is given by

$$\lambda = \frac{-\mu \pm \sqrt{\mu^2 - 8A}}{2}.$$

The eigenvalues of this matrix are either complex conjugate with negative real part or both negative real depending on μ . Therefore, $(\pm\sqrt{A/B}, 0)$ are either stable spirals or stable nodes of the system depending on μ . If the time-dependent part of the potential field vanishes, then the particle motion will stop after some time in one of the two minima of the potential. The remarkable behaviour of the dynamical system (5) can be understood by examining the interplay between the space-time-dependent field and the force due to double well potential.

2.2 Nonlinear damping

Case I

Now, we shall consider the motion of the particle under nonlinear damping and obtain the equation of motion

$$\ddot{x} = \mu\dot{x}(1 - x^2) - \alpha x - \beta x^3 + \frac{\omega^2 b}{2} \left[-\frac{b}{2} + \cos(\omega t) + \frac{b}{2} \cos(2\omega t) \right] x. \quad (10)$$

In the absence of oscillatory part we obtain

$$\ddot{x} - \mu\dot{x}(1 - x^2) - Ax + Bx^3 = 0, \quad (11)$$

where

$$A = -\left(\alpha + \frac{\omega^2 b^2}{4}\right), \quad B = \beta.$$

This is a Duffing–van der Pol-type equation. Equation (11) can be rewritten as

$$\begin{aligned} \dot{x} &= y \\ \dot{y} &= Ax - Bx^3 - \mu y(1 - x^2). \end{aligned} \quad (12)$$

The equilibrium points of the system are (0, 0) and $(\pm\sqrt{A/B}, 0)$. The Jacobian of system (12) is

$$J = \begin{pmatrix} 0 & 1 \\ A - 3Bx^2 - 2\mu xy & \mu(1 - x^2) \end{pmatrix}.$$

The value of the Jacobian matrix at (0, 0) is

$$J = \begin{pmatrix} 0 & 1 \\ A & \mu \end{pmatrix}.$$

Eigenvalue is given by

$$\lambda = \frac{\mu \pm \sqrt{\mu^2 + 4A}}{2}.$$

From our previous discussion we know $A > 0$. Therefore, the matrix has two real eigenvalues, one positive and one negative. Hence, the equilibrium point (0, 0) is a saddle point of system (12). The value of the Jacobian at $(\pm\sqrt{A/B}, 0)$ is

$$J = \begin{pmatrix} 0 & 1 \\ -2A & \mu(1 - (A/B)) \end{pmatrix}.$$

Eigenvalues of the above Jacobian matrix are given by

$$\lambda = \frac{\Delta_1 \pm \sqrt{\Delta_2}}{2}$$

where $\Delta_1 = \mu(B - A)$ and $\Delta_2 = \mu^2(B - A)^2 - 4AB^2$. Clearly, we can see that $\Delta_1 > \sqrt{\Delta_2}$. Now, if $\Delta_2 > 0$ then equilibrium point $(\pm\sqrt{A/B}, 0)$ becomes an unstable node for $B > A$ or a stable node for $B < A$. If $\Delta_2 < 0$, the equilibrium point becomes unstable spiral for $B > A$ or stable spiral for $B < A$. The behaviour of

the driven Duffing–van der Pol oscillator was reported earlier by Venkatesan and Lakshmanan [34].

Case II

$$\ddot{x} = -\mu\dot{x}|\dot{x}|^{p-1} - \alpha x - \beta x^3 + \frac{\omega^2 b}{2} \left[-\frac{b}{2} + \cos(\omega t) + \frac{b}{2} \cos(2\omega t) \right] x. \quad (13)$$

The nonlinear damping term is assumed to be proportional to the power of the velocity, in the form $\mu\dot{x}|\dot{x}|^{p-1}$ where $p \geq 1$ is the damping exponent and μ is the corresponding damping coefficient. In the absence of oscillatory part, we obtain

$$\ddot{x} + \mu\dot{x}|\dot{x}|^{p-1} - Ax + Bx^3 = 0, \quad (14)$$

where

$$A = -\left(\alpha + \frac{\omega^2 b^2}{4}\right), \quad B = \beta.$$

Equation (14) can be rewritten as

$$\begin{aligned} \dot{x} &= y \\ \dot{y} &= Ax - Bx^3 - \mu y|y|^{p-1}. \end{aligned} \quad (15)$$

The equilibrium points of the system are (0, 0) and $(\pm\sqrt{A/B}, 0)$. The Jacobian of system (15) is

$$J = \begin{pmatrix} 0 & 1 \\ A - 3Bx^2 & \mu[|y|^{p-1} + (p-1)y|y|^{p-2}\text{sgn}(y)] \end{pmatrix}. \quad (16)$$

The value of the Jacobian matrix at (0, 0) is

$$J = \begin{pmatrix} 0 & 1 \\ A & 0 \end{pmatrix}.$$

Eigenvalues are given by $\lambda = \pm\sqrt{A}$. As $A > 0$, the matrix has two real eigenvalues, one positive and one negative. Hence, the equilibrium point (0, 0) is a saddle point of system (15). The value of the Jacobian at $(\pm\sqrt{A/B}, 0)$ is

$$J = \begin{pmatrix} 0 & 1 \\ -2A & 0 \end{pmatrix}.$$

Eigenvalues of the above Jacobian matrix are given by $\lambda = \pm i\sqrt{2A}$, $A > 0$. So equilibrium point $(\pm\sqrt{A/B}, 0)$ becomes centre.

The effects of oscillating potential barrier is presented in the following section through numerical simulation results.

3. Numerical results

Nontrivial behaviours (limit cycle, quasiperiodic or chaotic oscillations) may occur due to the statistical

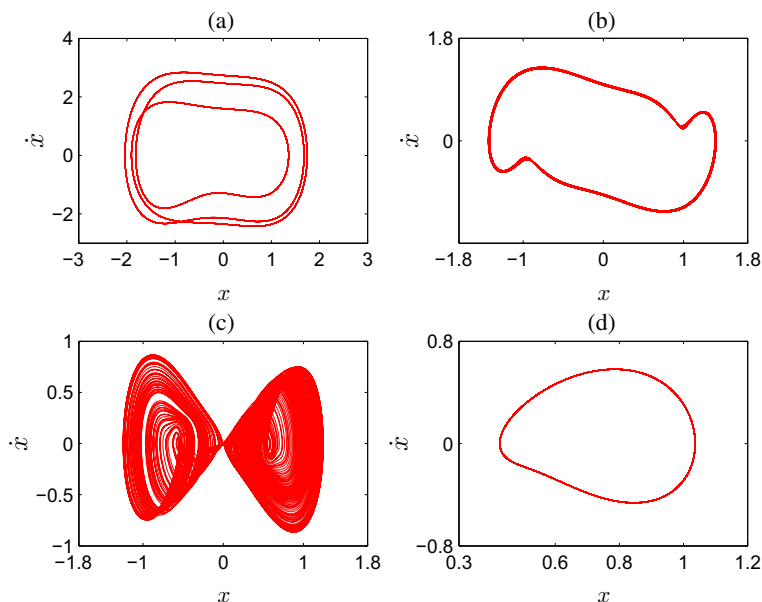


Figure 1. Phase portraits of the given system (6) in the $x\dot{x}$ plane for different values of μ : (a) period-3 ($\mu = 0.13$), (b) quasiperiodic ($\mu = 0.44$), (c) chaotic ($\mu = 1.0$) and (d) limit cycle ($\mu = 1.5$) when $\alpha = -1.6$, $\omega = 1.5$ and $b = 1.0$.

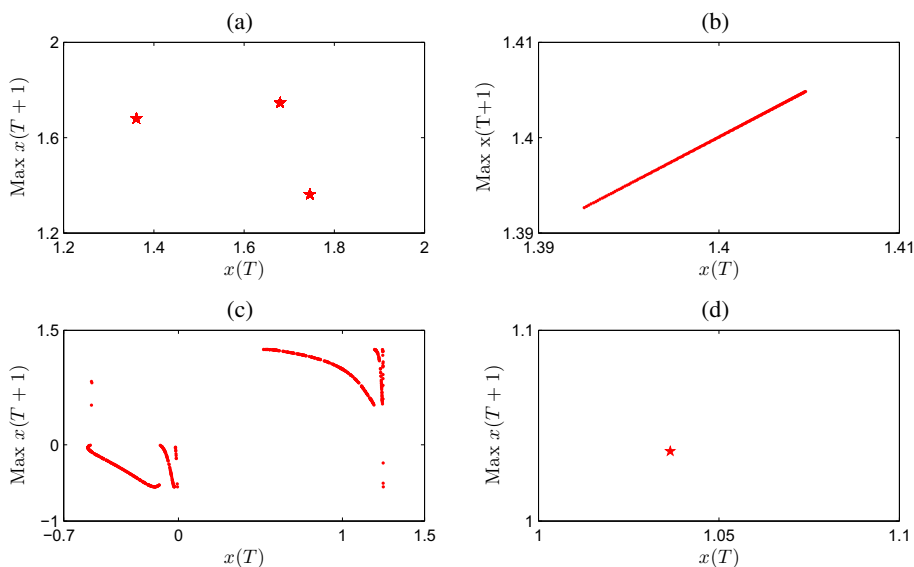


Figure 2. Poincaré return map of the given system (6) for different values of μ : (a) period-3 ($\mu = 0.13$), (b) quasiperiodic ($\mu = 0.44$), (c) chaotic ($\mu = 1.0$) and (d) limit cycle ($\mu = 1.5$) when $\alpha = -1.6$, $\omega = 1.5$ and $b = 1.0$ in the $x\dot{x}$ plane.

balance between dissipation and energy exchanges produced by the time-dependent potential. Indeed, the coupling of space–time-dependent potential with the background space-dependent potential yields an endogenous forcing term which allows a self-sustained unceasing motion, in the presence of friction. We solve system (6) numerically using fourth-order Runge–Kutta method starting with initial condition (0.04, 0.02, 0.1) and draw the phase portrait, bifurcation diagram and the variation of maximum Lyapunov exponent and Poincaré return map of the system for different sets of parameters. We

choose $\beta = -\alpha$ for numerical simulations of systems (6) and (13). We observe that there are no qualitative changes on the system dynamics when $|\beta| \neq |\alpha|$. We also do calculation for $\alpha < 0$ and $\beta > 0$ because in this case we get double-well potential.

Phase diagram of system (6) with $\alpha = -1.6$, $\omega = 1.5$ and $b = 1.0$ are shown in figure 1 for different values of μ in the $x\dot{x}$ plane. Figure 2 represents Poincaré return map while figure 3 represents bifurcation diagram and the corresponding maximum Lyapunov exponent of x with respect to parameter μ keeping the other

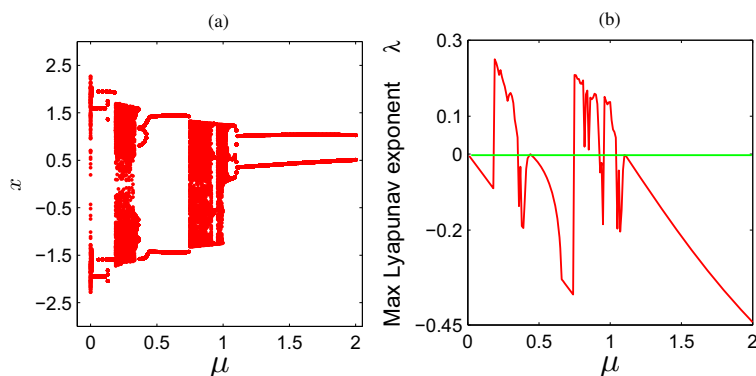


Figure 3. (a) Bifurcation diagram of x with respect to parameter μ and (b) variation of maximum Lyapunov exponent of system (6) with respect to parameter μ when $\alpha = -1.6$, $\omega = 1.5$ and $b = 1.0$.

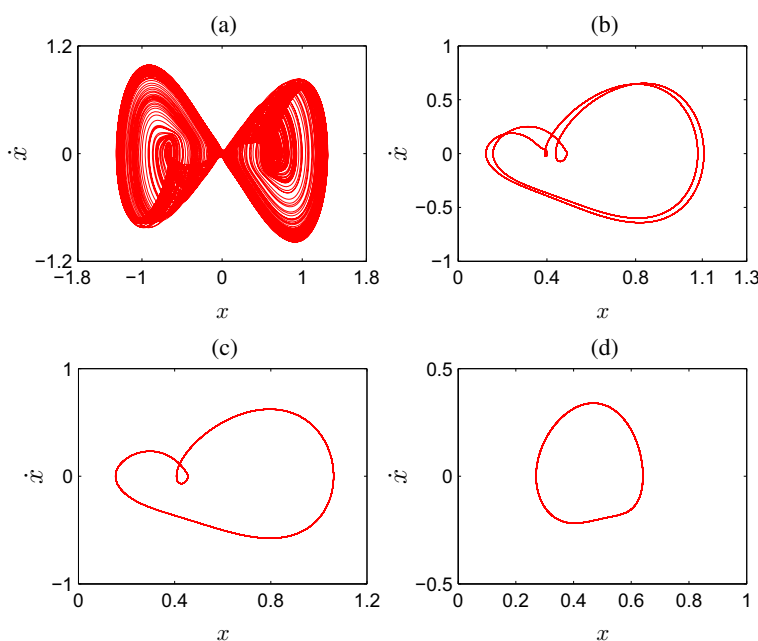


Figure 4. Phase portraits of the given system (6) in the $x\dot{x}$ plane for different values of α : (a) chaotic ($\alpha = -1.9$), (b) period-4 ($\alpha = -1.35$), (c) period-2 ($\alpha = -1.3$) and (d) limit cycle ($\alpha = -1.0$) when $\mu = 1.0$, $\omega = 1.5$ and $b = 1.0$.

parameters $\alpha = -1.6$, $\omega = 1.5$ and $b = 1.0$ fixed. In figure 1a, for $\mu = 0.13$ we notice period-3 orbit whose corresponding bifurcation diagram is presented in figure 3a. From figure 3b we observe that the maximum Lyapunov exponent becomes negative for $\mu = 0.13$. In figure 2a, we get three points which tell us that system (6) has periodic orbit for $\mu = 0.13$. Figure 1b shows quasiperiodic oscillation in the phase portrait for $\mu = 0.44$ while keeping the other parameters same as above. A smooth curve present in the Poincaré return map of x in figure 2b guarantees that system (6) shows quasiperiodic behaviour for $\mu = 0.44$. We notice that the corresponding largest Lyapunov exponent curve in figure 3b at $\mu = 0.44$ touches the green line which is at zero level. That means the maximum Lyapunov

exponent is equal to zero. Therefore, Poincaré return map, bifurcation diagram as well as maximum Lyapunov exponent curve altogether confirm that system (6) exhibits quasiperiodic behaviour for $\mu = 0.44$, $\alpha = -1.6$, $\omega = 1.5$ and $b = 1.0$. System (6) behaves chaotically for $\mu = 1.0$ in the $x\dot{x}$ plane with other parameters $\alpha = -1.6$, $\omega = 1.5$, $b = 1.0$ which is displayed in figure 1c. Poincaré return map in figure 2c shows the existence of lots of points at $\mu = 1.0$. In figure 3b, we observe that the corresponding maximum Lyapunov exponent becomes positive which guarantees the existence of chaos for $\mu = 1.0$. Phase portrait of system (6) for $\mu = 1.5$, $\alpha = -1.6$, $\omega = 1.5$ and $b = 1.0$ are shown in figure 1d. For $\mu = 1.5$, we observe from figure 3a that bifurcation diagram shows two points whereas the

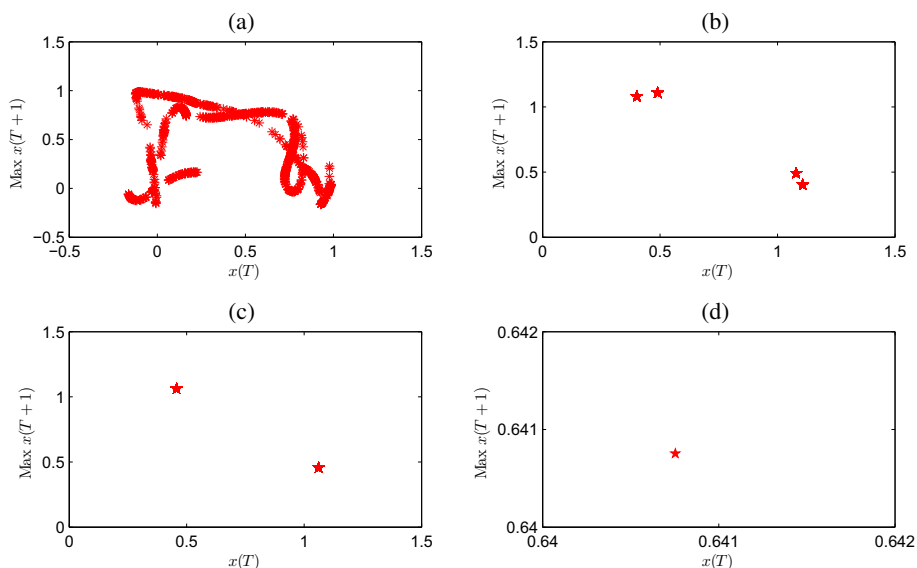


Figure 5. Poincaré return map plots of the given system (6) showing (a) chaotic ($\alpha = -1.9$), (b) period-4 ($\alpha = -1.35$), (c) period-2 ($\alpha = -1.3$) and (d) limit cycle ($\alpha = -1.0$) when $\mu = 1.0$, $\omega = 1.5$ and $b = 1.0$.

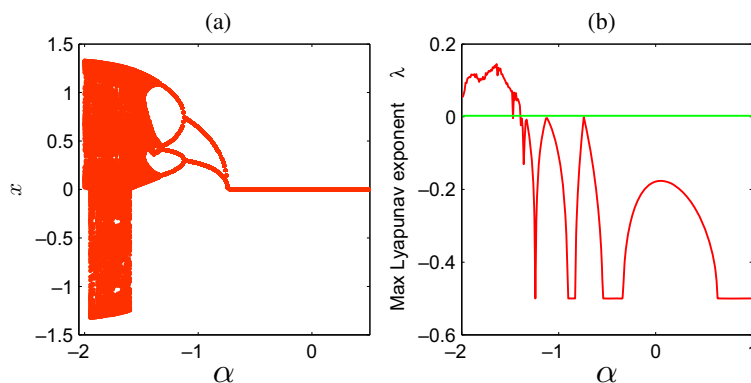


Figure 6. (a) Bifurcation diagram of x with respect to the parameter α and (b) variation of maximum Lyapunov exponent of system (6) with respect to parameter α for $\mu = 1.0$, $\omega = 1.5$ and $b = 1.0$.

maximum Lyapunov exponent becomes negative. Only one point present in the Poincaré return map of x for $\mu = 1.5$ which are drawn in figure 2d conclude that there are limit cycle in system (6) with the parameter $\mu = 1.5$, $\alpha = -1.6$, $\omega = 1.5$ and $b = 1.0$. Therefore, we observe periodic, quasiperiodic and chaotic behaviour of system (6) as we change the parameter μ in the $x\dot{x}$ plane keeping the other parameters fixed ($\alpha = -1.6$, $\omega = 1.5$ and $b = 1.0$).

In a similar way, we draw the phase portrait of system (6) in figure 4 by varying the parameter α keeping all other parameters fixed ($\mu = 1.0$, $\omega = 1.5$ and $b = 1.0$) in the $x\dot{x}$ plane. Figure 4a shows chaotic phase portrait while figures 4b, 4c and 4d display the periodic phase portrait with periodicity 4, 2 and 1 respectively. Figure 6 represents bifurcation diagram and the variation of the maximum Lyapunov exponent with respect to α .

Poincaré return maps are drawn in figure 5. We notice irregular set of points in figure 5a for $\alpha = -1.9$ which gives the conformity of the chaotic behaviour of system (6). We also observed 4, 2 and 1 points in the Poincaré return map presented in figures 5b, 5c and 5d respectively corresponding to $\alpha = -1.35$, $\alpha = -1.3$ and $\alpha = -1.0$. Poincaré return map guarantees that the phase portraits which are shown in figures 4b, 4c and 4d are period four orbit, two orbit and limit cycle respectively. Bifurcation diagram of x with respect to α is drawn in figure 6a keeping the other parameters fixed ($\mu = 1.0$, $\omega = 1.5$ and $b = 1.0$) which exhibits reverse period-doubling bifurcation. Maximum Lyapunov exponent curve presented in figure 6b satisfies all the above observations which are displayed in figures 4 and 5.

We depicted the phase portrait of system (6) by changing the value of ω keeping the other parameters $\mu = 0.5$,

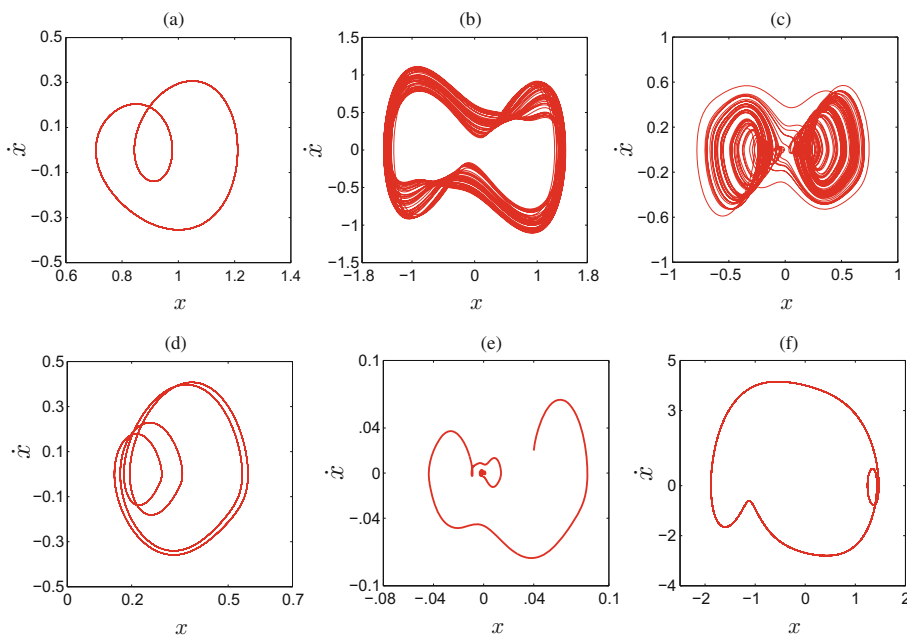


Figure 7. Phase portraits of the given system (6) in the $x\dot{x}$ plane for different values of ω . (a) Period-2 ($\omega = 0.8$), (b) quasiperiodic ($\omega = 1.2$), (c) chaotic ($\omega = 1.93$), (d) period-4 ($\omega = 1.96$), (e) stable node ($\omega = 2.5$), (f) period-2 ($\omega = 3.0$) when $\mu = 0.5$, $\alpha = -1.6$ and $b = 1.0$.

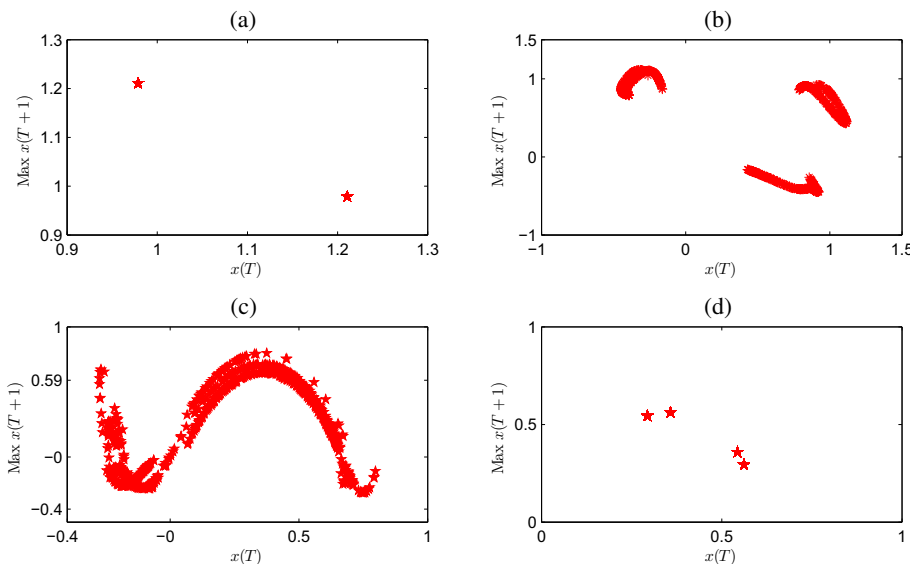


Figure 8. Poincaré return map plots of the given system (6) for different values of ω showing the existence of (a) period-2 ($\omega = 0.8$), (b) quasiperiodic ($\omega = 1.2$), (c) chaotic ($\omega = 1.93$) and (d) period-4 ($\omega = 1.96$) for $\mu = 0.5$, $\alpha = -1.6$ and $b = 1.0$.

$\alpha = -1.6$, $b = 1.0$ fixed in figure 7. Phase portrait in figure 7a is period 2 orbit for $\omega = 0.8$. We confirm it from its Poincaré return map presentation in figure 8a where we get two points. So the system shows periodic behaviour for $\omega = 0.8$. In figure 7b we observe quasiperiodic behaviour of system (6) for $\omega = 1.2$, while the Poincaré return map of the same is plotted in figure 8b. We observe that the Poincaré return map data

lie on three smooth closed curves confirming the existence of the quasiperiodic behaviour of the system. We have plotted the phase portrait for $\omega = 1.93$ in figure 7c. Poincaré return map corresponding to $\omega = 1.93$ which we display in figure 8c guarantees the existence of chaos in system (6). Again, system (6) exhibits periodic behaviour in phase plane $x\dot{x}$ for $\omega = 1.96$ and $\omega = 3.0$ which are displayed in figures 7d and 7f respectively. For

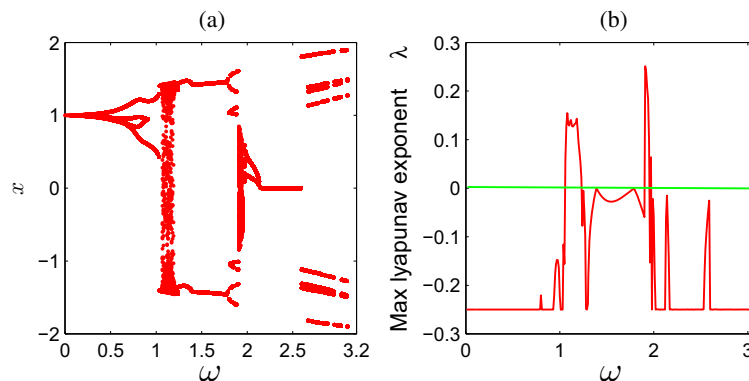


Figure 9. (a) Bifurcation diagram of x with respect to the parameter ω and (b) variation of the maximum Lyapunov exponent of system (6) with respect to parameter ω when $\mu = 0.5$, $\alpha = -1.6$ and $b = 1.0$.

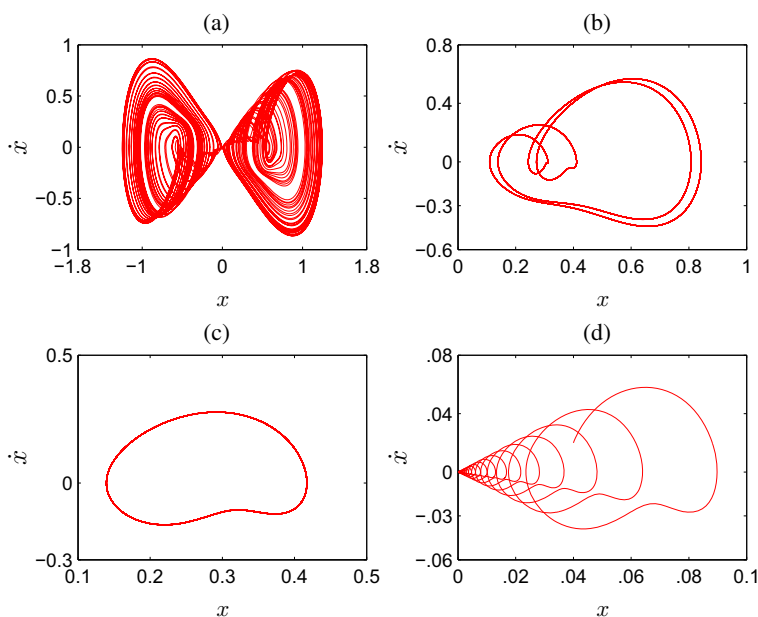


Figure 10. Phase portraits of the given system (6) in the $x\dot{x}$ plane for different values of b . (a) Chaotic ($b = 1.0$), (b) period-4 ($b = 1.27$), (c) limit cycle ($b = 1.4$) and (d) stable node ($b = 1.5$) when $\mu = 1.0$, $\alpha = -1.6$ and $\omega = 1.5$.

Poincaré return map for $\omega = 1.96$, we get finite number of points which we display in figure 8d. When $\omega = 2.5$, $\mu = 0.5$, $\alpha = -1.6$, $b = 1.0$, the phase portrait in figure 7e are stable node, i.e., the whole system contracted towards the origin. Bifurcation diagram and the corresponding maximum Lyapunov exponent are drawn in figure 9 and we get satisfactory result compared to the above phase portrait.

Again we vary another parameter b and we capture phase portrait, bifurcation diagram and maximum Lyapunov exponent of system (6) when $\mu = 1.0$, $\alpha = -1.6$ and $\omega = 1.5$ in figures 10, 11 and 12 respectively. We observed that system (6) shows chaotic behaviour for $b = 1.0$, periodic behaviour for $b = 1.27$ (period 4) and limit cycle for $b = 1.4$. We found a drastic change

in system (6) for $b = 1.5$ where we notice that the whole system contracted to a stable node. In a similar way, Poincaré return map, bifurcation diagram as well as maximum Lyapunov exponent curve, all satisfy the above claim. Here we also observed reverse period doubling bifurcation in figure 12a in the region $b = 1.0$ to $b = 2.0$.

Next, we summarized the phase portrait, Poincaré return map and bifurcation diagram of system (10) in figures 13, 14 and 15 respectively varying the parameter α while the other parameters remain constant at $\mu = 0.5$, $\beta = 0.5$, $\omega = 1.5$ and $b = 1.0$. Figure 13a shows period 3 orbit for $\alpha = -1.0$ and its corresponding Poincaré return map is drawn in figure 14a which shows three points. Therefore, we conclude that

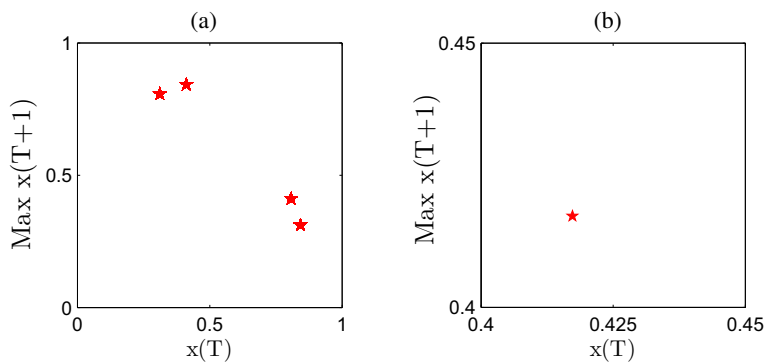


Figure 11. Phase portraits of the given system (6) for different values of b . (a) Period-4 ($b = 1.27$) and (b) limit cycle ($b = 1.4$) when $\mu = 1.0$, $\alpha = -1.6$ and $\omega = 1.5$ in the $x\dot{x}$ plane.

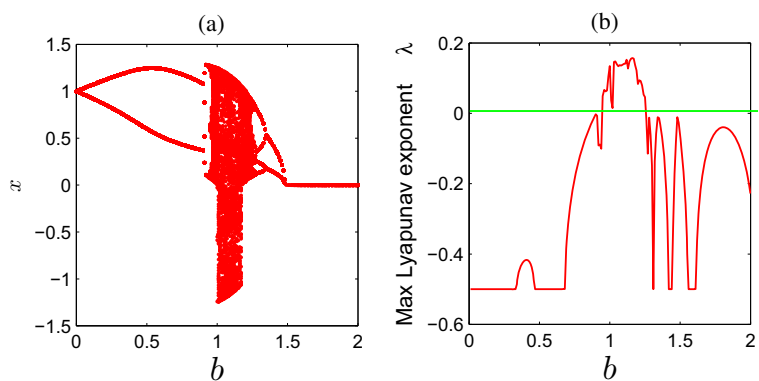


Figure 12. (a) Bifurcation diagram of x with respect to parameter b and (b) variation of the maximum Lyapunov exponent of system (6) with respect to parameter b when $\mu = 1.0$, $\alpha = -1.6$ and $\omega = 1.5$.

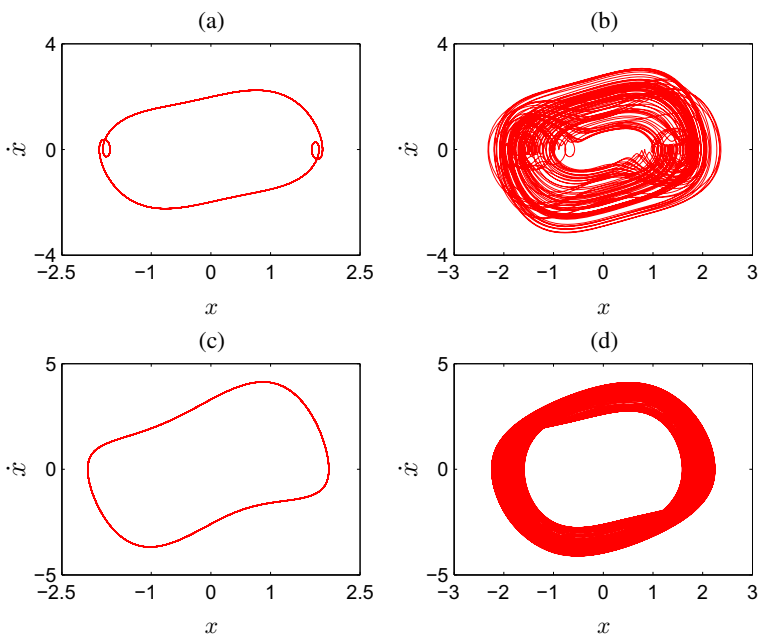


Figure 13. Phase portraits of the given system (10) in the $x\dot{x}$ plane for different values of α . (a) Period-3 ($\alpha = -1.0$), (b) chaotic ($\alpha = -0.6$), (c) limit cycle ($\alpha = 0.2$) and (d) quasiperiodic ($\alpha = 1.5$) choosing $\mu = 0.5$, $\beta = 0.5$, $\omega = 1.5$ and $b = 1.0$.

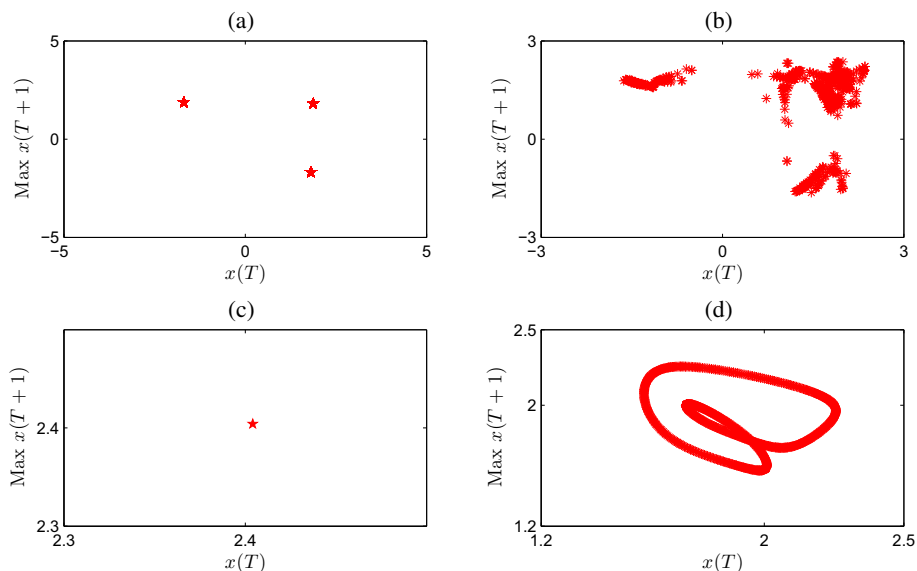


Figure 14. Phase portraits of the given system (10) for different values of α . (a) Period-3 ($\alpha = -1.0$), (b) chaotic ($\alpha = -0.6$), (c) limit cycle ($\alpha = 0.2$) and (d) quasiperiodic ($\alpha = 1.5$) when $\mu = 0.5$, $\beta = 0.5$, $\omega = 1.5$ and $b = 1.0$ in the $x\dot{x}$ plane.

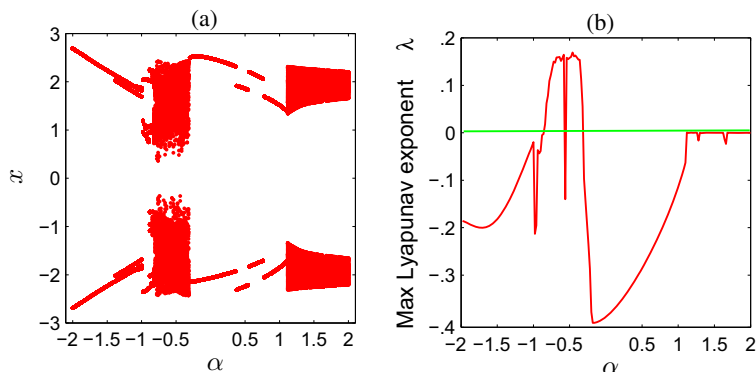


Figure 15. (a) Bifurcation diagram of x with respect to parameter α and (b) variation of the maximum Lyapunov exponent of system (10) with respect to parameter α when $\mu = 0.5$, $\beta = 0.5$, $\omega = 1.5$ and $b = 1.0$.

system (10) shows regular behaviour for $\alpha = -1.0$. We have plotted the phase portrait for $\alpha = -0.6$ in figure 13b and the corresponding return map data are plotted in figure 14b. The irregular set of points in the whole plane guarantees the existence of chaos in the system for $\alpha = -0.6$. Phase portrait for $\alpha = 0.2$ and the corresponding Poincaré first return map are shown in figures 13c and 14c respectively. The existence of only one point in figure 14c proves the existence of limit cycle. In figure 13d, the phase diagram of the system is plotted for $\alpha = 1.5$ and the corresponding Poincaré return map is shown in figure 14d. The return map data lie on the smooth closed curves and hence confirm the existence of quasiperiodic behaviour of the system for $\alpha = 1.5$. Bifurcation diagram and the corresponding maximum Lyapunov exponent curve also satisfy the above result.

Again we consider eq. (13) and we can see for $p = 1$, this system is equivalent to system (6). Here p is our parameter and we want to see the effect of p in our system. We describe the phase diagram of system (13) taking the parameters $\mu = 1.0$, $\alpha = -1.6$, $\omega = 1.5$, $b = 1.0$ fixed in the $x\dot{x}$ plane for $p = 1.0$ in figure 16a whereas for $p = 2.5$ in figure 16b. We get chaotic picture for $p = 1.0$ where we get limit cycle for $p = 2.5$. Poincaré return map for $\mu = 1.0$, $p = 1.0$ keeping other parameters the same as above is drawn in figure 17a. The irregular scattering of points in the figure points to the existence of chaos in the system. Only one point in the Poincaré return map of x shown in figure 17b for $\mu = 1.0$, $p = 2.5$ guarantees that the system has a limit cycle. So, as parameter p changes from 1.0 to 2.5, the system dynamics also changes from chaotic to periodic. Here,

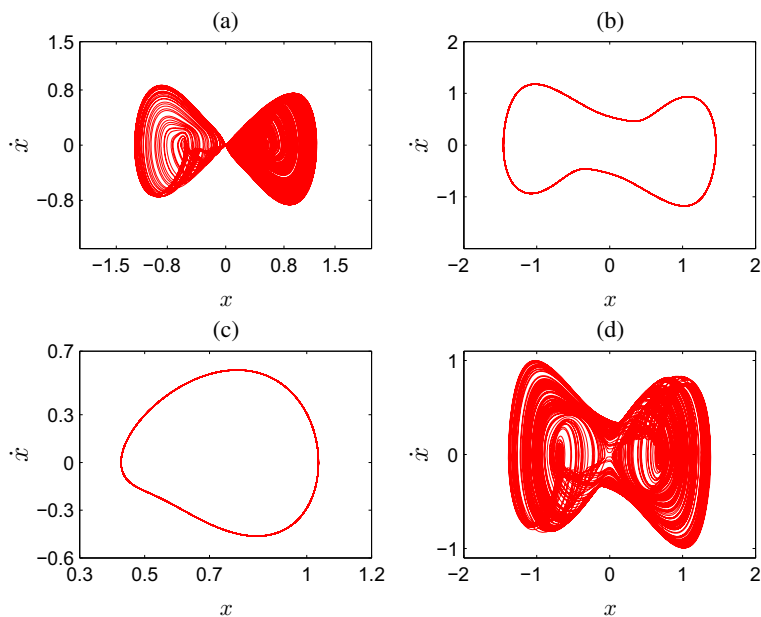


Figure 16. Phase portraits of the given system (13) in the $x\dot{x}$ plane for different values of p . (a) Chaotic ($p = 1.0, \mu = 1.0$), (b) limit cycle ($p = 2.5, \mu = 1.0$), (c) limit cycle ($p = 1.0, \mu = 1.5$) and (d) chaotic ($p = 2.5, \mu = 1.5$) when $\alpha = -1.6, \omega = 1.5$ and $b = 1$.

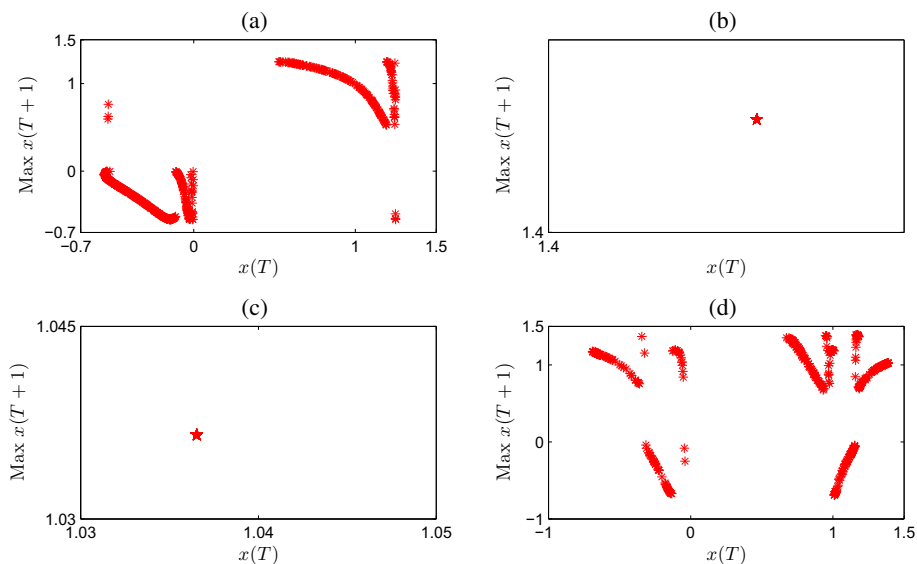


Figure 17. Phase portraits of the given system (13) for different values of p . (a) Chaotic ($p = 1.0, \mu = 1.0$), (b) limit cycle ($p = 2.5, \mu = 1.0$), (c) limit cycle ($p = 1.0, \mu = 1.5$) and (d) chaotic ($p = 2.5, \mu = 1.5$) when $\alpha = -1.6, \omega = 1.5$ and $b = 1$ in the $x\dot{x}$ plane.

p plays the role of control parameter which can control chaotic dynamics of the system. The phase diagram of the system for $\mu = 1.5, \alpha = -1.6, \omega = 1.5, b = 1.0$ with $p = 1.0$ and $p = 2.5$ are depicted in figure 16c and figure 16d respectively. From the corresponding Poincaré return map (figure 17c) we conclude that there are periodic orbit of system (13) for $\mu = 1.5, p = 1.0$. We find a set of randomly distributed points in figure

17d that tells us about the chaotic character inherent in system (13) for $\mu = 1.5, p = 2.5$. So, as the value of p increases, the system dynamics also changes from periodic to chaotic. Here, the parameter p plays the role of the controller. Therefore, the parameter p plays a significant role in the dynamics of system (13). In figures 18a and 18b, we represent bifurcation diagram of x with respect to p for $\mu = 1.0$ and $\mu = 1.5$ respectively.

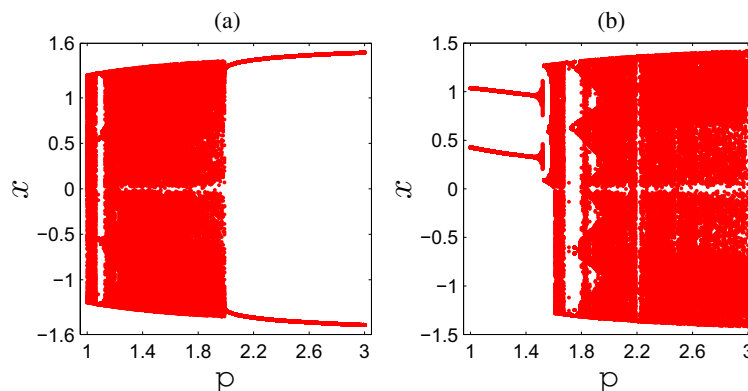


Figure 18. Bifurcation diagram of x with respect to parameter p when $\alpha = -1.6$, $\omega = 1.5$ and $b = 1.0$ for (a) $\mu = 1.0$ and (b) $\mu = 1.5$ of system (13).

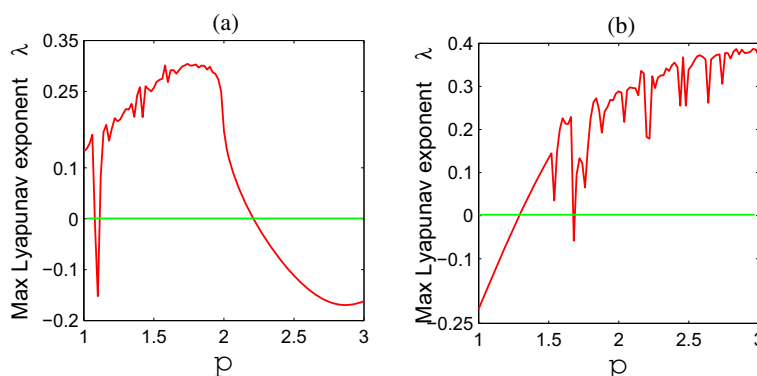


Figure 19. Variation of maximum Lyapunav exponent of with respect to parameter p when $\alpha = -1.6$, $\omega = 1.5$ and $b = 1.0$ for (a) $\mu = 1.0$ and (b) $\mu = 1.5$ for system (13).

Variation of maximum Lyapunov exponent of system (13) with respect to parameter p keeping $\alpha = -1.6$, $\omega = 1.5$, $b = 1.0$ fixed for $\mu = 1.0$ and $\mu = 1.5$ are drawn in figure 19. Bifurcation diagram as well as maximum Lyapunov exponent graph satisfy the above result.

4. Conclusions

We have investigated the classical dynamics of a particle moving inside an oscillating potential well. We found that the motion of such a particle depends significantly on the initial state of the particle in some region of the physical parameter space. It is shown that stable limit cycle oscillation is possible in such an oscillating potential field. The corresponding dynamics can be interpreted as the one-dimensional motion of a particle in a potential well with oscillating barrier subjected to a viscous damping and time-dependent forcing. Forcing is essential for chaos because it acts

as an endogenous forcing which is able to permanently sustain the motion in the presence of viscous damping. Typical nonlinear behaviours, including limit cycle, quasiperiodic and chaotic oscillations, may take place due to the statistical balance between dissipation and energy exchanges produced by the time-dependent potential. Indeed, the coupling of space–time-dependent potential with the background space-dependent potential yields an endogenous forcing term which allows a self-sustained unceasing motion, in the presence of viscous damping. We can control the chaotic motion of the system either by increasing the viscous damping or controlling the frequency of oscillation of the potential barrier.

References

[1] M Festa, A Mazzino and D Vincenzi, *Phys. Rev. E* **65**, 046205 (2002)
 [2] M Lakshmanan *et al*, *Phys. Rev. E* **61**, 3641 (2000)

- [3] M Lakshmanan and K Murali, *Chaos in nonlinear oscillators: Synchronization and controlling* (World Scientific, Singapore, 1996)
- [4] M Lakshmanan, *Nonlinear dynamics: Integrability, chaos, and patterns* (Springer, Berlin, 2003)
- [5] M Lakshmanan, *Pramana – J. Phys.* **64**, 617 (2005)
- [6] M Leng and C S Lent, *Phys. Rev. Lett.* **71**, 137 (1993)
- [7] G A Luna-Acosta, G Orellana Rivadeneyra, A Mendoza-Galvn and C Jung, *Chaos, Solitons and Fractals* **12**, 349 (2001)
- [8] D R da Costa, C P Dettmann and E D Leonel, *Phys. Rev. E* **83**, 066211 (2011)
- [9] O Farago and Y Kantor, *Physica A* **249**, 151 (1998)
- [10] P S S Guimares *et al*, *Phys. Rev. Lett.* **70**, 3792 (1993)
- [11] M Buttiker and R Landauer, *Phys. Rev. Lett.* **49**, 1739 (1982)
- [12] E D Leonel and P V E McClintock, *Phys. Rev. E* **70**, 016214 (2004)
- [13] J L Mateos and J V Jos, *Physica A* **257**, 434 (1998)
- [14] J L Mateos, *Phys. Lett. A* **256**, 113 (1999)
- [15] E D Leonel and J K L da Silva, *Physica A* **323**, 181 (2003)
- [16] A J Lichtenberg and M A Lieberman, Regular and chaotic dynamics, in: *Applied mathematical science* (Springer, New York, 1992) Vol. 38
- [17] M Tabor, *Chaos and integrability in nonlinear dynamics: An introduction* (Wiley, New York, 1989)
- [18] M V Berry, *Eur. J. Phys.* **2**, 91 (1981)
- [19] G Karner, *J. Stat. Phys.* **77**, 867 (1994)
- [20] K Y Tsang and K L Ngai, *Phys. Rev. E* **56**, R17 (1997)
- [21] S Rajendran, P Muruganandam and M Lakshmanan, *Physica D* **227**, 1 (2007)
- [22] V Berdichevsky and M Gitterman, *Phys. Rev. E* **59**, R9 (1999); *J. Phys. A* **29**, L447 (1996)
- [23] D Dragoman and M Dragoman, *Quantum-classical analogies* (Springer, Berlin, 2004)
- [24] J N Bandyopadhyay, A Lakshminarayan and V B Sheorey, *Phys. Rev. A* **63**, 042109 (2001)
- [25] Lewis H Ralph and P G L Leach, *J. Math. Phys.* **23**, 165 (1982)
- [26] P Camiz, A Gerardi, C Marchioro, E Presutti and E Scaciatelli, *J. Math. Phys.* **12**, 2040 (1971)
- [27] D Laroze, G Gutierrez, R Rivera and Julio M Ynez, *Phys. Scr.* **78**, 015009 (2008)
- [28] A Sharma, V Patidar, G Purohit and K K Sud, *Commun. Nonlinear Sci. Numer. Simulat.* **17**, 2254 (2012)
- [29] D V Parshin, I V Ufimtseva, A A Cherevko, A K Khe, Orlov K Yu, A L Krivoschapkin and A P Chupakhin, *J. Phys.: Conf. Ser.* **722**, 012030 (2016)
- [30] P Ghorbaniana, S Ramakrishnana, A Whitmanb and H Ashrafiuona, *Biomed. Signal Process. Control* **15**, 1 (2015)
- [31] A Ridinger and N Davidson, *Phys. Rev. A* **76**, 013421 (2007)
- [32] B Hutcheon and Y Yarom, *Trends Neurosci. (TINS)* **23**, 216 (2000)
- [33] J Belmonte-Beitia and G Calvo, *Phys. Lett. A* **373**, 448 (2009)
- [34] A Venkatesan and M Lakshmanan, *Phys. Rev. E* **56**, 6321 (1997)